Sputtering-induced Co^0 formation in x-ray photoelectron spectroscopy of nanocrystalline $Zn_{1-x}Co_xO$ spinodal enrichment models

Michael A. White,[1,3] Tracy C. Lovejoy,[2,3] Stefan T. Ochsenbein,[1,3] Marjorie A. Olmstead,[2,3] and Daniel R. Gamelin[1,3,a)]
[1]*Department of Chemistry, University of Washington, Seattle, Washington 98195, USA*
[2]*Department of Physics, University of Washington, Seattle, Washington 98195, USA*
[3]*The Center for Nanotechnology, University of Washington, Seattle, Washington 98195, USA*

(Received 25 February 2010; accepted 25 March 2010; published online 25 May 2010)

Nanoscale enrichments resulting from spinodal decomposition have been proposed to contribute to the interesting magnetic properties of diluted magnetic oxides such as cobalt-doped ZnO ($Zn_{1-x}Co_xO$), but little is known experimentally about the electronic structures or physical properties of such enrichments. Here, x-ray photoelectron spectroscopy (XPS) is used to examine wurtzite $Zn_{1-x}Co_xO$ crystallites over the full composition range ($0.0 \leq x \leq 1.0$) that serve as models of the proposed spinodal decomposition nanostructures within $Zn_{1-x}Co_xO$ bulk materials. With increasing x, the valence band edge shifts to smaller binding energies and the cobalt $2p$ peaks shift to greater binding energies, providing spectroscopic signatures that may allow identification of spinodal decomposition in bulk $Zn_{1-x}Co_xO$. Reduction of Co^{2+} to Co^0 by argon ion (Ar^+) sputtering was also found to become markedly more facile with increasing x, suggesting that locally-enriched $Zn_{1-x}Co_xO$ is at greater risk of yielding false-positive Co^0 XPS signals than uniformly dilute $Zn_{1-x}Co_xO$ with the same overall composition. © *2010 American Institute of Physics*.
[doi:10.1063/1.3407517]

I. INTRODUCTION

The magnetic properties of the diluted magnetic semiconductor (DMS) $Zn_{1-x}Co_xO$ and related oxides continue to be intensely investigated.[1] Various synthetic techniques and post-synthetic treatments have generated materials that are nominally the same yet show strikingly different magnetic properties. In some instances strong correlations between ferromagnetism and the reversible introduction of charge carriers by Zn vapor annealing[2–5] or electrical gating[6] have been observed. Heavily n-doped $Zn_{1-x}Co_xO$ films of high structural quality show no ferromagnetism, however, indicating that carriers alone are not sufficient to activate ferromagnetism.[7] Reconciling these differences, several experiments have implicated grain boundaries in the activation of such oxide ferromagnetism,[8–11] but the relevant grain-boundary defects and their associated bound charge carriers have been challenging to explore thoroughly, either experimentally or theoretically.

One hypothesis proposed to explain the curious robustness of the ferromagnetism of high-temperature ferromagnetic DMSs such as $Zn_{1-x}Co_xO$ invokes the notion that spinodal decomposition enhances magnetic correlations by increasing local magnetic ion concentrations (x_{loc}).[12–15] Spinodal decomposition alone does not appear to generate ferromagnetism in $Zn_{1-x}Co_xO$,[16,17] but it is conceivable that it could be a necessary-but-not-sufficient condition, e.g., with donor defects also required for high-T_C ferromagnetism. Difficulties arise in the investigation of spinodal decomposition in $Zn_{1-x}Co_xO$ because of the similar local electronic and geometric environments of Co^{2+} and Zn^{2+} in the wurtzite lattice.

A second frequently proposed hypothesis is that the ferromagnetism of this entire class of materials, and of $Zn_{1-x}Co_xO$ in particular, arises from undetected cobalt metal or cobalt/zinc intermetallic precipitates embedded within the sample matrix, because in some cases such inclusions have been detected.[18,19] As a universal explanation, this hypothesis is also problematic because, as noted in Ref. 18, the quantities of metallic impurities detected by extended x-ray-absorption fine structure (EXAFS) do not appear to correlate with the magnitudes of the ferromagnetic saturation moments of the same samples. Whereas the EXAFS measurements in Ref. 18 show a large metallic Co^0 EXAFS feature for a film with small (0.05 μ_B/Co) room-temperature ferromagnetism, parallel EXAFS measurements on a $Zn_{1-x}Co_xO$ film having two times stronger ferromagnetism (0.10 μ_B/Co) failed to expose any detectable metallic impurity.[3] Experimentally verifying the metallic inclusion hypothesis thus requires methods that reliably detect metal inclusions *and* demonstrate their correlation with the observed ferromagnetism. A powerful technique widely applied for detecting metallic inclusions is x-ray photoelectron spectroscopy (XPS), which is sensitive to changes in dopant charge state and to local electronic structure perturbations within a given charge state. Because XPS is a surface technique, it is usually used in conjunction with argon ion (Ar^+) sputtering, which removes surface carbon and can be used for depth proiling. XPS has recently provided key evidence supporting the hypothesis of metal inclusions as a common origin of $Zn_{1-x}Co_xO$ ferromagnetism.[7,20] As with EXAFS, however, Co^0 XPS peak intensities do not correlate with ferromagnetism as expected. Very large Co^0 peaks were observed by XPS in Ref. 18 (0.05 μ_B/Co) but not in Ref. 5 (up

a)Electronic mail: gamelin@chem.washington.edu.

 © 2010 American Institute of Physics

Author complimentary copy. Redistribution subject to AIP license or copyright, see http://jap.aip.org/jap/copyright.jsp

to 0.03 μ_B/Co), despite exposure to Zn vapor in both studies.

In this study, we have examined $Zn_{1-x}Co_xO$ nanocrystal models of the hypothesized spinodal decomposition nanostructures using XPS. Colloidal $Zn_{1-x}Co_xO$ nanocrystals were prepared at various values of x to mimic the different compositions expected in a film that has undergone the proposed spinodal decomposition. By this approach, the properties of the enriched nanostructures can be examined without contributions from the bulk regions of such a film. Optical, magnetic, and magneto-optical trends across this composition series have already been reported elsewhere.[16] The data presented here show differences in XPS results between the similar tetrahedral Co^{2+} ions of dilute (small x_{loc}) and concentrated (large x_{loc}) wurtzite $Zn_{1-x}Co_xO$. In the process of these experiments, however, it was furthermore observed that Ar^+ sputtering of Co^{2+}-enriched $Zn_{1-x}Co_xO$ leads to formation of Co^0 with disproportionate ease, even under mild sputtering conditions. This latter result demonstrates an unexpected relationship between two of the leading hypotheses for magnetic ordering of oxide DMSs: wurtzite $Zn_{1-x}Co_xO$ samples with local enrichments in Co^{2+} (e.g., from spinodal decomposition) are evidently far more likely to show metallic Co^0 peaks in their XPS spectra than samples with uniformly distributed Co^{2+} ions, even when no Co^0 was actually present prior to the XPS experiment, because of inadvertent Co^{2+} reduction during Ar^+ sputtering. Because Co^0 formation occurs only in the XPS probe region, which is a small fraction of the total sample, the *apparent* Co^0 content determined by XPS bears little resemblance to the actual Co^0 content of the sample. This observation tempers the assertion that XPS can be used as an unambiguous probe of trace metallic inclusions in $Zn_{1-x}Co_xO$ and related doped oxides.

II. EXPERIMENTAL

Wurtzite $Zn_{1-x}Co_xO$ nanocrystals with nominal Co^{2+} concentrations of x=0.00, 0.0075, 0.05, 0.10, 0.40, 0.90, and 1.00 were grown and characterized as described in detail previously.[16] To reach the composition of x=0.90 in $Zn_{1-x}Co_xO$, which has never been reported previously, 0.05 g of Co(acetylacetonate)$_2$ and 0.005 g Zn(acetylacetonate)$_2$ were added to 7.6 g degassed oleylamine at 135 °C. This solution was stirred and heated to 200 °C for 30 min. The nanocrystals that formed were then cooled quickly to 90 °C with a water bath, and washed repeatedly by precipitation and centrifugation with ethanol followed by re-suspension in toluene.

As prepared, all of these nanocrystals are easily dispersed in toluene or other organic solvents to provide colloidal suspensions of high optical quality. Transmission electron microscopy (TEM) images and electron diffraction images were collected with a FEI Tecnai G2 F20 transmission electron microscope at the UW Center for Nanotechnology User Facility. Magnetic measurements were collected with a Quantum Design MPMS-5 superconducting quantum interference device magnetometer on sealed air-free colloidal suspensions in frozen toluene at 2 K. The sample diamagnetism

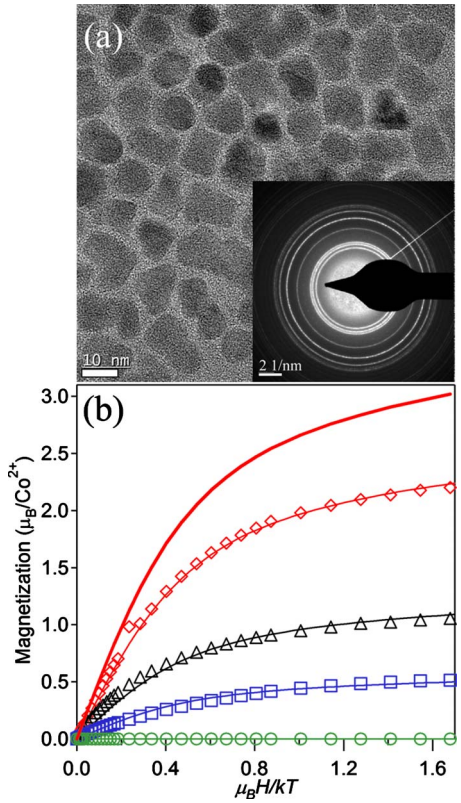

FIG. 1. (Color online) (a) TEM image of x=1.00 (w-CoO) nanocrystals. The scale bar is 10 nm. The electron diffraction pattern shown in the inset reveals the wurtzite structure of these nanocrystals. (b) 2 K magnetization for x=0.0075 (red diamonds), 0.05 (black triangles), 0.40 (blue squares), and 1.00 (green circles) samples (data adapted from Ref. 16). The solid lines show calculated 2 K powder magnetization curves for paramagnetic Co^{2+} in the wurtzite lattice structure with various values of x_{eff}.

was estimated from the linear component of the room-temperature magnetization for each sample and subtracted from the 2 K data.

Samples for XPS measurements were prepared by depositing the colloidal crystallites onto transparent conductive fluorine-doped tin oxide substrates, which were then inserted into a commercial XPS instrument (PHI VersaProbe) that uses monochromatic aluminum K_α excitation (1486 eV) and a hemispherical capacitor analyzer with an overall resolution of 0.6 eV (full width at half maximum on Au 4f). Charge neutralization was carried out for all measurements using simultaneous electron and Ar^+ flood guns with accelerating voltages of 10 V and 30 V, respectively. Argon ion sputtering consisted of rastering 0.5 kV Ar^+ ions over a 2×2 mm^2 area at an angle of 45° for 30 s, repeated six times with two-minute wait periods between cycles. These conditions yielded a sputtering rate of 1.6 nm/min (calibrated to SiO_2). The same sputtering parameters were applied for all samples.

III. RESULTS

A. TEM and Magnetism

A TEM image of the as-prepared x=1.00 nanocrystals is shown in Fig. 1(a). An average nanocrystal diameter of ~10–20 nm is estimated for these and the other samples of this study. The inset of Fig. 1(a) shows the wurtzite electron

Author complimentary copy. Redistribution subject to AIP license or copyright, see http://jap.aip.org/jap/copyright.jsp

diffraction pattern obtained from a ~1.0 μm spot diameter. Low-temperature magnetization data collected for colloidal suspensions of $Zn_{1-x}Co_xO$ nanocrystals at four representative values of x are shown in Fig. 1(b). The solid lines in Fig. 1 show the 2 K powder-averaged magnetization calculated using the axial spin Hamiltonian in Eq. (1) for paramagnetic Co^{2+}. In these calculations, the ground-state spin $S=3/2$, the axial zero-field splitting energy $D=2.72\ cm^{-1}$, and the quasi-isotropic Landé g factor of $g=2.27$, are taken from literature studies of bulk wurtzite $Zn_{1-x}Co_xO$.[21,22] The thick solid line shows the calculated magnetization of isolated Co^{2+} ions in wurtzite ZnO (no antiferromagnetic nearest-neighbor coupling). The data show a reduction in the average magnetic moment per cobalt ion with increasing x, which is attributed to antiferromagnetic coupling between nearest neighbor magnetic ions,[16,17] and allow the conclusion that Co^{2+} substitution in these nanocrystals is reasonably close to statistical,[16] as expected. The good agreement between the calculated and experimental results over the entire range of x, and in particular the absence of any hysteresis or indication of superparamagnetism in the low-field region, eliminates the possibility of metallic Co^0 as a contaminant phase in these samples. The absence of Co^0 is not surprising given the oxidative conditions of the nanocrystal syntheses, and is corroborated by the absence of highly contrasting metallic nanocrystals in TEM images of these samples [e.g., Fig. 1(a)]

$$\mathcal{H} = D\left[\hat{S}_z^2 - \frac{1}{3}S(S+1)\right] + g\mu_\beta \mathbf{SH}. \quad (1)$$

B. XPS

Figure 2(a) shows the valence band XPS spectra of several $Zn_{1-x}Co_xO$ powder samples of varying x. To the best of our knowledge, the XPS spectrum of wurtzite CoO (w-CoO, $x=1.00$) has not been reported previously. All spectra were aligned at the O 1s XPS binding energy at 530.4 eV, which is known to arise from oxygen at a ZnO lattice site.[18,20,23] A second oxygen peak observed at slightly higher energy (~532 eV) has been assigned as surface oxygen or hydroxide.[20] These O 1s peaks do not shift or broaden significantly with increasing x.

At small x, Co^{2+} doping introduces new intensity ~1.5 eV shallower than the ZnO valence band, consistent with previous results.[24–26] This impurity intensity grows and shifts to lower binding energies as x is increased. Over the same series of samples, the Zn 3d XPS intensity (at ~10 eV) diminishes with increasing x before disappearing at $x=1.00$. Figure 2(b) shows the XPS spectrum of the $x=0.05$ sample (black line) plotted along with the spin-resolved total density of states (gray line) and cobalt partial density of states (filled, ×10) for $Zn_{1-x}Co_xO$ ($x=0.006$), calculated by density functional theory and adapted from Ref. 27. The calculated binding energies were shifted to align with the experimental spectrum in the ZnO valence band region. The good overall agreement between experimental

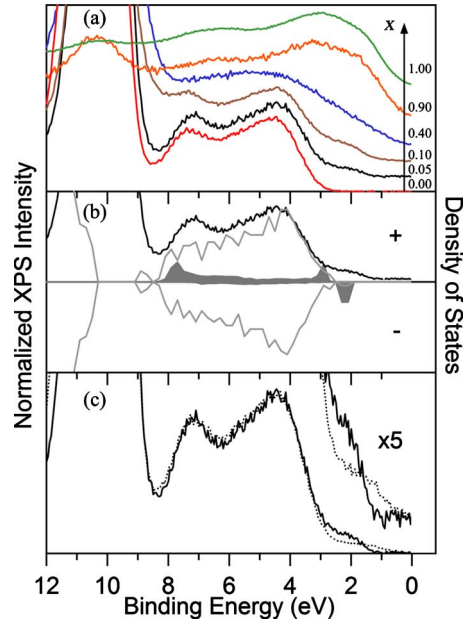

FIG. 2. (Color online) XPS data for the valence band and Zn 3d region of $Zn_{1-x}Co_xO$ crystallites. (a) Data for $x=0.00$ (red), 0.05 (black), 0.10 (brown), 0.40 (blue), 0.90 (orange), and 1.00 (green) samples, normalized to the O 2p peak maximum and offset for clarity. (b) Comparison of the valence band XPS spectrum for $x=0.05$ (black) with the spin-resolved total density of states (gray) and Co^{2+} partial density of states (filled, ×10) calculated by density functional theory for $x=0.006$ (adapted from Ref. 27). The increasing intensity above the top of the ZnO valence band with increasing x is due to occupied Co^{2+} 3d levels. (c) XPS spectrum for $x=0.05$ (solid curve) and sum of the XPS spectra for $x=0.00$ and $x=1.00$ weighted to yield x_{avg} ~0.05 (dotted line, x_{loc} ~1.0).

and calculated results [Fig. 2(c)] confirms association of the new XPS intensity above the valence band maximum with the occupied Co^{2+} 3d levels.

The presence of Co^{2+} d levels above the valence band edge also impacts the optical spectroscopy. The optical transition involving promotion of these same Co^{2+} 3d electrons into the ZnO conduction band has been identified ~1.5 eV below the ZnO band-to-band transition (3.4 eV),[28,29] in excellent agreement with the Co^{2+} XPS intensity that is ~1.5 eV above the ZnO valence band maximum [Fig. 2(b)]. Interestingly, optical data suggest that w-CoO is a charge-transfer insulator, with an optical band gap (2.3 eV) determined by the O^{2-} (2p)-to-Co^{2+} (3d) charge-transfer energy.[16] If this material were instead a Mott insulator, the band-gap excitation would have metal-to-metal charge-transfer character, but such transitions are estimated to occur at much higher energies (~5–6 eV) (Ref. 30) than the experimental optical gap of w-CoO.[16] The data in Fig. 2(a) thus suggest the presence of localized Co^{2+} 3d levels at the top of an O 2p-derived valence band in w-CoO.

The data in Fig. 2(a) indicate that XPS can be used to distinguish between two samples with similar x but different x_{loc}, for example, between a $Zn_{1-x}Co_xO$ film with a statistical dopant distribution and one that has undergone spinodal decomposition. This distinction is illustrated in Fig. 2(c), which compares data for the $x=0.05$ (x_{loc} ~0.05, i.e., approximately statistical) sample with the simulated spectrum of an x ~0.05 (x_{loc} ~1.00, i.e., simulated spinodal decomposition) sample having the same integrated Co^{2+} 3d intensity, ob-

Author complimentary copy. Redistribution subject to AIP license or copyright, see http://jap.aip.org/jap/copyright.jsp

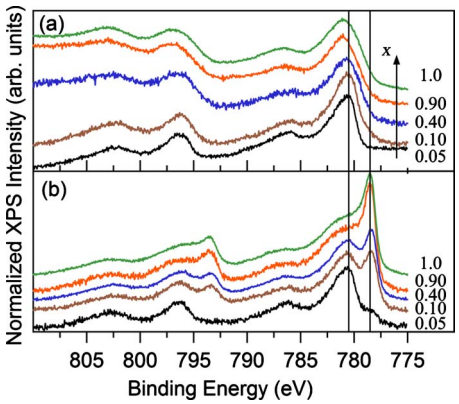

FIG. 3. (Color online) (a) Normalized Co $2p$ XPS data for $x=0.05$ (black), 0.10 (brown), 0.40 (blue), 0.90 (orange), and 1.00 (green) $Zn_{1-x}Co_xO$ crystallites collected without sputtering. The Co^{2+} $2p_{3/2}$ and $2p_{1/2}$ peaks shift to higher binding energies with increasing x. The lines at 778.5 and 780.7 eV are guides to the eye. The spectra are normalized to the Co^{2+} $2p_{3/2}$ intensity at 781 eV and offset for clarity. (b) Spectra of the same series of samples collected after Ar^+ sputtering, showing increasing Co^0 intensity with increasing x (sharp peaks at 778.5 and 793.5 eV). The Co^0 intensity is an artifact of the Ar^+ sputtering process, which itself causes reduction of Co^{2+} to form Co^0.

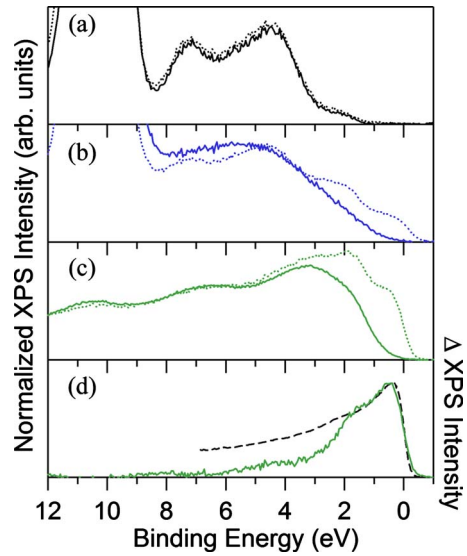

FIG. 4. (Color online) Normalized valence band XPS spectra collected before (solid) and after (dotted) sputtering for $x=$(a) 0.05, (b) 0.40, and (c) 1.0 $Zn_{1-x}Co_xO$ crystallites. (d) The difference between before and after sputtering for the $x=1.0$ sample (green solid), and an experimental Co^0 XPS spectrum (black dashed, adapted from Ref. 34). The Co^0 intensity is an artifact of the Ar^+ sputtering process, which itself causes reduction of Co^{2+} to form Co^0.

tained from a linear combination of $x=1.00$ and 0.00 spectra of Fig. 2(a). For the same average x, there is a clear shift in the onset of Co^{2+} $3d$ ionization by ~0.8 eV to lower binding energy from small x_{loc} to large x_{loc}. This comparison suggests that the valence band region of the XPS spectrum may be useful for identification of spinodal decomposition in $Zn_{1-x}Co_xO$ films.

Figure 3(a) shows Co $2p$ XPS spectra of the samples from Fig. 2. The spectra at small x agree well with previous results.[5,20,31] Cobalt $2p_{3/2}$ (780.5 eV) and $2p_{1/2}$ (796.2 eV) peaks are observed, as are shake-up satellites that indicate high-spin Co^{2+}.[20,31,32] Notably, there is no peak at 778.5 eV that would be indicative of Co^0,[20] consistent with the magnetic results [Fig. 1(b)]. Increasing x from 0.05 to 1.00 broadens the Co^{2+} peaks and shifts them by ~0.3 eV to higher binding energy. These changes are interpreted as reflecting greater inelastic scattering losses at large x, possibly due to short-range magnetic coupling. The shift of the Co^{2+} $2p$ peak to higher binding energy (Fig. 3) and of the valence band to lower binding energy (Fig. 2) with increasing x are both manifestations of x-dependent Co^{2+} electronic structural changes that could be useful for identification of spinodal segregation by XPS in other forms of $Zn_{1-x}Co_xO$.

C. Ar^+ sputtering

The data discussed above were all collected without Ar^+ sputtering, which is commonly used to remove carbon impurities and the top few nanometers of a sample surface, either to increase XPS intensities or for depth profiling. In this section we describe how XPS spectra collected following relatively mild Ar^+ sputtering of the same samples discussed above yield completely different results, and how these results are artifacts of the sputtering process and not accurate representations of the true materials composition.

It has already been shown[33] that sputtering cubic CoO at 5 kV for 2 h can create Co^0, so the conditions used here were substantially more gentle. Ar^+ ions were rastered at 0.5 kV for a total exposure of 6 min (see Sec. II). The XPS data collected following sputtering are presented in Fig. 3(b), in comparison with those collected on the same samples before sputtering [Fig. 3(a)]. The ZnO and small-x $Zn_{1-x}Co_xO$ samples showed little change with sputtering, the main effects being a loss of C $1s$ intensity, a loss of the higher-energy (surface) O $1s$ intensity, and an increase in all other intensities, consistent with previous observations.[20,31,33] At higher x, however, two new sharp peaks appeared at 778.5 and 793.5 eV that are readily associated with Co^0.[20] At $x=1.00$, far more Co^0 is detected than Co^{2+}, no matter where on the sputtered sample the XPS is probed. This composition is entirely inconsistent with magnetic and TEM measurements of the same samples prior to sputtering (Fig. 1). Because these other measurements preclude the prior existence of metallic Co^0 in these nanocrystals, let alone as the major component as would be suggested by Fig. 3(b) for large x, the appearance of these new Co^0 peaks only following sputtering are indicative of sputter reduction in Co^{2+} to Co^0. The small Co^0 satellite peaks anticipated at ~4 eV higher binding energy[7] are presumably also present but occluded by the Co^{2+} $2p$ peaks. Importantly, the intensities of these sputter-induced Co^0 peaks relative to the Co^{2+} peaks are *strongly* dependent upon the initial Co^{2+} concentration, with a larger fraction of Co^{2+} being reduced at higher x [Fig. 3(b)]. We emphasize that sputter reduction occurs only in the small region of the powder sample that has been sputtered, and does not accurately reflect the true composition of the material in areas that have not been sputtered.

Sputtering generates new features in the valence band energy region as well, again strongly dependent upon x. Figure 4 shows data for three representative samples before (solid) and after (dashed) sputtering. Whereas the $x=0.05$

Author complimentary copy. Redistribution subject to AIP license or copyright, see http://jap.aip.org/jap/copyright.jsp

sample [Fig. 4(a)] shows little change, the samples with greater x [Figs. 4(b) and 4(c)] show new metallic states in the oxide band gap following sputtering. This new intensity is correlated with the Co^0 intensity at 778.5 eV from Fig. 3(b), and matches the density of states of cobalt metal. Fig. 4(d) illustrates this similarity by plotting the difference between XPS spectra collected before and after sputtering for the $x=1.0$ nanocrystals (solid line) along with the valence band XPS spectrum of a metallic Co^0 film (dashed line, adapted from Ref. 34). Together, the introduction of metallic states at the Fermi level and growth of the Co^0 $2p$ intensity upon sputtering indicate that sputter reduction of Co^{2+} to Co^0 is greatly facilitated at higher x. The formation of Co^0 is attributed to the preferential sputtering of oxygen under these conditions; when elemental oxygen is removed from the lattice, the two remaining electrons reduce Co^{2+} to Co^0. This formation of Co^0 may occur at a lattice site, but since the formation of Co^0 may be facilitated by movement through the ZnO lattice, the Co^0 may be preferentially created in a metallic phase. There is not enough experimental evidence to distinguish between these two possibilities. The observation of Co^0 by XPS does not necessarily implicate the formation of metallic Co^0 clusters or CoZn intermetallics, because Co^0 could also exist in a dilute form, for example, at interstitial sites within the ZnO lattice. Although metallic cluster formation appears most likely, the present data cannot eliminate the latter possibility.

We emphasize that this Co^0 XPS intensity is a *consequence* of Ar^+ sputtering, but could easily have been misinterpreted as evidence of metallic impurities in these samples. These observations thus have bearing on the evaluation of metallic impurity contamination and other hypotheses for understanding the ferromagnetism of $Zn_{1-x}Co_xO$, and by extension also related DMSs. The data here clearly demonstrate that Co^{2+} enrichment greatly increases the propensity for Co^0 formation by sputter reduction in $Zn_{1-x}Co_xO$. A similar sputter reduction process could very well lead to false-positive identification of Co^0 by XPS in samples that contained no metallic impurity prior to the XPS experiment, but instead showed only local Co^{2+} enrichment that possibly arose from spinodal decomposition. Such a false-positive identification of Co^0 would lead to very different interpretation of any observed magnetism, and moreover would lead to detected Co^0 levels that showed no correlation with ferromagnetism because they were artifacts of the measurement. It is impossible to know whether such false positives have been previously reported, but the results presented here draw attention to the possibility.

Figure 5 summarizes these findings schematically: when x_{loc} is small, sputter-induced Co^0 formation is not prominent, but when x_{loc} is large, sputter-induced Co^0 formation becomes markedly more facile. Whereas these results have been obtained using $Zn_{1-x}Co_xO$ nanocrystals in which x is varied to model degrees of spinodal enrichment [Fig. 5(b)], similar sputter reduction can reasonably be expected in thin films [Fig. 5(a)]. Indeed, 4 kV Ar^+ sputtering of $Zn_{1-x}Co_xO$ ($x=0.30$) films for 5 min reportedly revealed similar new Co^0 XPS features that were not observed prior to sputtering,[20] and the data here support the possibility that those features were artifacts derived from the sputter process itself rather than from prior existence of extensive metallic Co^0 inclusions in the internal volume of the film.

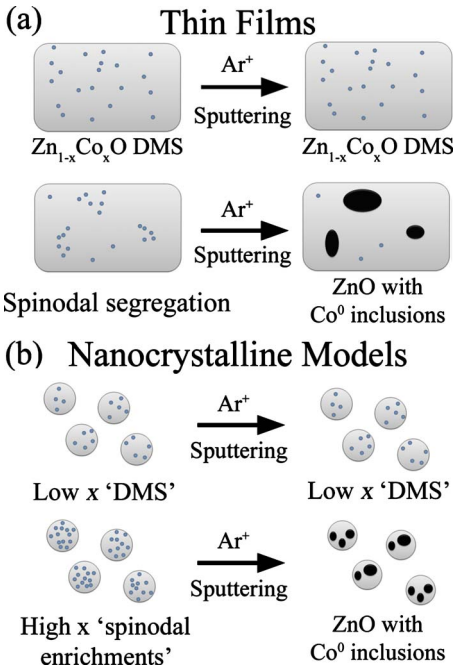

FIG. 5. (Color online) The effect of Ar^+ sputtering on various $Zn_{1-x}Co_xO$ samples. (a) $Zn_{1-x}Co_xO$ thin films or macrocrystals with spinodal Co^{2+} enrichments (large x_{loc}) may yield false-positive Co^0 XPS signals when sputtering is used to prepare their surfaces. (b) For the $Zn_{1-x}Co_xO$ crystallites studied here, sputtering causes little or no change in cobalt speciation when x is small, but Co^{2+} reduction to form Co^0 becomes increasingly facile for increasing x, eventually leading to strong false-positive Co^0 XPS signals.

IV. SUMMARY

XPS spectra of $Zn_{1-x}Co_xO$ ($0.0 \leq x \leq 1.0$) nanocrystals prepared to model spinodal enrichments in $Zn_{1-x}Co_xO$ show shifts in the Co $2p$ and valence band ionization energy regions with increasing x that can be related to changes in Co^{2+} electronic structure. These spectral shifts may prove helpful in the detection of spinodal decomposition in thin films and other forms of $Zn_{1-x}Co_xO$. The data also reveal a strong dependence of the *observation* of metallic Co^0 by XPS on x in wurtzite $Zn_{1-x}Co_xO$, despite the absence of any Co^0 in these samples prior to the XPS measurement: Increasing x strongly facilitates sputtering reduction of Co^{2+} ions to form Co^0 in the XPS probe region, even under mild sputtering conditions. This relationship between x and ease of Co^{2+} sputter reduction could potentially lead to false identification of metallic Co^0 inclusions in samples that actually possess only enrichments of Co^{2+} (i.e., large x_{loc}). Overall, these data provide new information about the electronic structures of highly Co^{2+}-enriched wurtzite $Zn_{1-x}Co_xO$, and demonstrate the characterization of such phases by XPS. The demonstration of sputter reduction dependent on x in $Zn_{1-x}Co_xO$ has bearing on evaluation of the role of Co^0 inclusions in the high-temperature ferromagnetism of this and related oxide DMSs.

This work was funded by NSF Grant Nos. CRC-0628252 (DRG) and DMR-0605601 (MAO, TCL). MAW

Author complimentary copy. Redistribution subject to AIP license or copyright, see http://jap.aip.org/jap/copyright.jsp

was supported through the UW-CNT as an NSF/NCI IGERT trainee (Grant No. DGE-0504573). The authors thank Professor Xiaosong Li and Ekaterina Badaeva for sharing the DFT results. The XPS instrumentation was funded by the Micron Foundation.

[1]S. J. Pearton, D. P. Norton, M. P. Ivill, A. F. Hebard, J. M. Zavada, W. M. Chen, and I. A. Buyanova, IEEE Trans. Electron Devices **54**, 1040 (2007).
[2]D. A. Schwartz and D. R. Gamelin, Adv. Mater. **16**, 2115 (2004).
[3]K. R. Kittilstved, D. A. Schwartz, A. C. Tuan, S. M. Heald, S. A. Chambers, and D. R. Gamelin, Phys. Rev. Lett. **97**, 037203 (2006).
[4]N. Khare, M. J. Kappers, M. Wei, M. G. Blamire, and J. L. MacManus-Driscoll, Adv. Mater. **18**, 1449 (2006).
[5]L. R. Shah, H. Zhu, W. G. Wang, B. Ali, T. Zhu, X. Fan, Y. Q. Song, Q. Y. Wen, H. W. Zhang, S. I. Shah, and J. Q. Xiao, J. Phys. D **43**, 035002 (2010).
[6]H.-J. Lee, E. Helgren, and F. Hellman, Appl. Phys. Lett. **94**, 212106 (2009).
[7]T. C. Kaspar, T. Droubay, S. M. Heald, P. Nachimuthu, C. M. Wang, V. Shutthanandan, C. A. Johnson, D. R. Gamelin, and S. A. Chambers, New J. Phys. **10**, 055010 (2008).
[8]P. V. Radovanovic and D. R. Gamelin, Phys. Rev. Lett. **91**, 157202 (2003).
[9]T. C. Kaspar, S. M. Heald, C. M. Wang, J. D. Bryan, T. Droubay, V. Shutthanandan, S. Thevuthasan, D. E. McCready, A. J. Kellock, D. R. Gamelin, and S. A. Chambers, Phys. Rev. Lett. **95**, 217203 (2005).
[10]P. I. Archer and D. R. Gamelin, J. Appl. Phys. **99**, 08M107 (2006).
[11]T. C. Kaspar, T. Droubay, V. Shutthanandan, S. M. Heald, C. M. Wang, D. E. McCready, S. Thevuthasan, J. D. Bryan, D. R. Gamelin, A. J. Kellock, M. F. Toney, X. Hong, C. H. Ahn, and S. A. Chambers, Phys. Rev. B **73**, 155327 (2006).
[12]T. Dietl, T. Andrearczyk, A. Lipinska, M. Kiecana, M. Tay, and Y. Wu, Phys. Rev. B **76**, 155312 (2007).
[13]T. Fukushima, K. Sato, H. Katayama-Yoshida, and P. H. Dederichs, Jpn. J. Appl. Phys., Part 2 **45**, L416 (2006).
[14]K. Sato, T. Fukushima, and H. Katayama-Yoshida, Jpn. J. Appl. Phys., Part 2 **46**, L682 (2007).
[15]K. Sato, H. Katayama-Yoshida, and P. H. Dederichs, Jpn. J. Appl. Phys., Part 2 **44**, L948 (2005).
[16]M. A. White, S. T. Ochsenbein, and D. R. Gamelin, Chem. Mater. **20**, 7107 (2008).
[17]R. Hanafin, T. Archer, and S. Sanvito, Phys. Rev. B **81**, 054441 (2010).
[18]T. C. Kaspar, T. Droubay, S. M. Heald, M. H. Engelhard, P. Nachimuthu, and S. A. Chambers, Phys. Rev. B **77**, 201303(R) (2008).
[19]J. H. Park, M. G. Kim, H. M. Jang, S. Ryu, and Y. M. Kim, Appl. Phys. Lett. **84**, 1338 (2004).
[20]M. Ivill, S. J. Pearton, S. Rawal, L. Leu, P. Sadik, R. Das, A. F. Hebard, M. Chisholm, J. D. Budai, and D. P. Norton, New J. Phys. **10**, 065002 (2008).
[21]W. H. Brumage, C. F. Dorman, and C. R. Quade, Phys. Rev. B **63**, 104411 (2001).
[22]P. Koidl, Phys. Rev. B **15**, 2493 (1977).
[23]J. Haber, K. Kosinski, and M. Rusiecka, Faraday Discuss. Chem. Soc. **58**, 151 (1974).
[24]M. Kobayashi, Y. Ishida, J. L. Hwang, T. Mizokawa, A. Fujimori, K. Mamiya, K. Okamoto, Y. Takeda, T. Okane, Y. Saitoh, Y. Muramatsu, A. Tanaka, H. Saeki, H. Tabata, and T. Kawai, Phys. Rev. B **72**, 201201(R) (2005).
[25]S. C. Wi, J. S. Kang, J. H. Kim, S. B. Cho, B. J. Kim, S. Yoon, B. J. Suh, S. W. Han, K. H. Kim, K. J. Kim, B. S. Kim, H. J. Song, H. J. Shin, J. H. Shim, and B. I. Min, Appl. Phys. Lett. **84**, 4233 (2004).
[26]S. C. Wi, J.-S. Kang, J. H. Kim, S. S. Lee, S.-B. Cho, B. J. Kim, S. Yoon, B. J. Suh, S. W. Han, K. H. Kim, K. J. Kim, B. S. Kim, H. J. Song, H. J. Shin, J. H. Shim, and B. I. Min, Phys. Status Solidi B **241**, 1529 (2004).
[27]E. Badaeva, Y. Feng, D. R. Gamelin, and X. Li, New J. Phys. **10**, 055013 (2008).
[28]W. K. Liu, G. M. Salley, and D. R. Gamelin, J. Phys. Chem. B **109**, 14486 (2005).
[29]C. A. Johnson, T. C. Kaspar, S. A. Chambers, G. M. Salley, and D. R. Gamelin, Phys. Rev. B **81**, 125206 (2010)
[30]J. van Elp, J. L. Wieland, H. Eskes, P. Kuiper, G. A. Sawatzky, F. M. F. de Groot, and T. S. Turner, Phys. Rev. B **44**, 6090 (1991).
[31]A. C. Tuan, J. D. Bryan, A. B. Pakhomov, V. Shutthanandan, S. Thevuthasan, D. E. McCready, D. Gaspar, M. H. Engelhard, J. W. Rogers, Jr., K. Krishnan, D. R. Gamelin, and S. A. Chambers, Phys. Rev. B **70**, 054424 (2004).
[32]D. C. Frost, C. A. McDowell, and I. S. Woolsey, Mol. Phys. **27**, 1473 (1974).
[33]T. Choudhury, S. O. Saied, J. L. Sullivan, and A. M. Abbot, J. Phys. D **22**, 1185 (1989).
[34]L. E. Klebanoff, D. G. Van Campen, and R. J. Pouliot, Phys. Rev. B **49**, 2047 (1994).

Author complimentary copy. Redistribution subject to AIP license or copyright, see http://jap.aip.org/jap/copyright.jsp